Highlights

How low must the freezing limit of a nitrate salt be? Freeze-protection cost sets the oil–salt parity boundary for cold-site parabolic-trough plants

Zhaohui Han, Zengli Dai, Yuan Wei, Yu Xie, Dongxiang Wang

- Electric freeze protection costs a Solar Salt trough 206 MWh/yr vs 6 MWh for oil
- Air-pressure effects at 2801 m change annual output by only 0.1%
- Salt matches oil once its minimum operating temperature falls to about 197°C
- Parity temperature and optimal storage shift with storage cost and accounting
- A 170–500°C ternary-like window is 4.7% cheaper than the oil reference

How low must the freezing limit of a nitrate salt be? Freeze-protection cost sets the oil–salt parity boundary for cold-site parabolic-trough plants

Zhaohui Han[a,*], Zengli Dai[a], Yuan Wei[a], Yu Xie[a], Dongxiang Wang[a]

[a] *SEPCOIII Electric Power Construction Co., Ltd., Qingdao, 266100, Shandong, China*

Abstract

Molten nitrate salt lets parabolic-trough plants deliver heat at 540°C and store it directly, but at cold sites the receiver inventory must be kept above its freezing limit whenever the field is not collecting. This study asks how low that limit must be for a direct Solar-Salt plant to match a thermal-oil plant with indirect salt storage. A one-loop equivalent plant at Golmud, China (2801 m; annual DNI 1898 kWh m^{-2}) is simulated hourly with a segmented receiver enthalpy model, an explicit storage ledger, three receiver-maintenance policies and separate grid import and export accounts. With steady electric maintenance, salt needs 206 MWh of heating electricity per year against 6 MWh for oil; its net-energy levelized cost rises from 739 to 906 CNY MWh^{-1}, above the 846 CNY MWh^{-1} of oil. A fixed-weather pressure experiment changes annual output by only 0.1%, so the penalty comes from the freeze-protection burden rather than from air density. With storage re-optimised over hourly candidates, salt reaches parity once its minimum operating temperature falls to 196.5°C. Across 98 storage-cost and accounting combinations, 61 give a parity temperature between 90 and 240°C, and the cost-optimal storage moves between 0 and 7 h. A ternary-salt-like window of 170–500°C gives 804 CNY MWh^{-1}, 4.7% below oil, which would tolerate a salt price of about 10.8 CNY kg^{-1} in the storage inventory. The results give salt developers a quantitative freezing-limit target and show which operating and accounting assumptions move it.

Keywords: parabolic trough, molten salt, freeze protection, heat-transfer fluid, thermal energy storage, levelized cost

*Corresponding author.
Email address: hanzhaohui@sepco3.com (Zhaohui Han)

1. Introduction

Parabolic troughs are the most mature concentrating collector technology[1]. Most parabolic-trough plants use synthetic oil as the heat-transfer fluid (HTF), which limits the field outlet to about 400°C and requires an oil–salt heat exchanger when the plant has molten-salt storage[2, 3, 4]. Using nitrate salt in the field removes that exchanger, raises the delivery temperature and stores the field fluid directly[5, 6, 7]. The penalty is the salt's high freezing limit: Solar Salt ($NaNO_3$–KNO_3, 60–40 wt%) solidifies at roughly 220–240°C, so every receiver, header and pipe must be kept warm, drained or reheated when the sun is not available[5, 8, 9]. China has built much of its recent concentrating solar power capacity on cold, high-altitude sites in Qinghai and Gansu[10, 11], where this penalty is paid on most nights of the year.

Operating experience with salt-filled trough loops is growing. The Évora molten-salt platform has run a 3.5 MW_{th} trough with a ternary salt between about 180 and 500°C and reports preheating, draining and cold-spot management as central operating tasks[12]; loop-wise flow control has been tested on the same platform[13]. Laboratory work has measured solidification and melting of Solar Salt in evacuated and non-evacuated receiver tubes[14], and tank design practice for molten-salt storage is well documented[15, 16]. These studies show that freeze protection is an engineering cost that recurs throughout plant life, not a one-off design detail.

Materials research aims to reduce that cost by lowering the freezing limit. Quaternary nitrate mixtures[17], binary to quaternary nitrate phase diagrams[18], quinary nitrate/nitrite mixtures[19] and lithium-containing mixtures[20] report melting values well below that of Solar Salt. These studies also show why one temperature cannot describe a salt: melting onset, liquidus and crystallisation on cooling differ by tens of kelvin, and the upper stability limit often falls when the lower limit falls[17, 19]. A material developer therefore needs a system-level target. The question is how low the usable minimum temperature must be before a salt-HTF plant becomes cheaper than an oil plant at a given site, and how that target depends on storage, operating policy and cost.

The closest system study is that of Dersch et al.[21], who compared VP-1 oil, Solar Salt and a ternary salt in parabolic-trough plants at three sunny sites with several storage capacities. In their model, freeze protection draws on stored heat first and then on natural-gas auxiliary heating; electric freeze protection was not considered. They found the ternary salt to give the lowest levelized cost at all three sites; Solar Salt beat oil clearly at the high-DNI Moroccan site, but at the

other two sites only with more than 12 h of storage. Energy–exergy–economic–environmental studies of trough systems have examined other configurations and fluids[22, 23, 24]. Altitude effects have been studied for flat-plate collectors[25], and receiver heat-loss models have been reviewed[26]. None of these studies expresses the oil–salt comparison at a cold site as a required freezing limit.

This study fills that gap for a cold, high-altitude site with electric freeze protection (Table 1). It makes four contributions. First, a fixed-weather pressure experiment separates the effect of air density on receiver heat loss from the effect of freeze protection. Second, three receiver-maintenance policies and two electricity-accounting conventions are compared on one hourly ledger with separate grid import and export. Third, the comparison is expressed as a parity minimum operating temperature, with storage re-optimised over hourly candidates and the target mapped over 49 storage-cost combinations. Fourth, a ternary-salt-like operating window and a raw-material inventory check translate the target into a cost allowance that material developers can use.

Table 1: Scope of this study compared with the closest prior system study.

Aspect	Dersch et al. 2025[21]	This study
Fluids	VP-1 oil, Solar Salt, ternary salt	VP-1 oil, Solar Salt, ternary-salt-like window
Sites	Three sunny sites (Morocco, United Arab Emirates, Spain)	Golmud, China: 2801 m, 2550 h below 0°C in the TMY
Freeze protection	Stored heat first, then natural-gas auxiliary; electric heating not modelled	Electric steady maintenance, thermal inertia with start-up debit, and stored-heat supply
Electricity accounting	Net generation	Hourly import and export, net-energy and export-based levelized cost
Storage	Several capacities (capacity factors 0.3–0.8)	0–12 h in 1 h steps, re-optimised for each cost case
Main output	Levelized cost ranking by site and storage	Parity minimum operating temperature and cost allowance over 98 cost and accounting cases

2. Methods

Figure 1 shows the two plant configurations and the boundaries of the energy ledger. Both plants share the same site, weather, collector loop and power-block model; they differ in HTF, field temperatures, storage arrangement and freeze-protection demand.

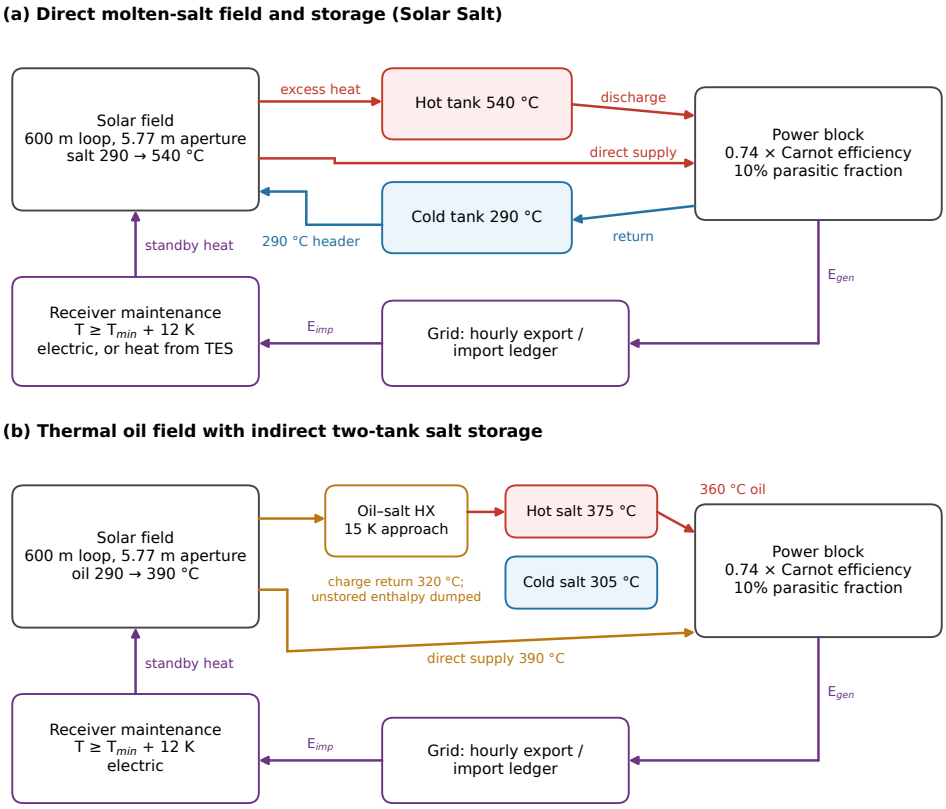


Figure 1: System boundaries. (a) Direct molten-salt plant: the field heats Solar Salt from 290 to 540°C and charges a two-tank store directly. (b) Oil plant: the field heats VP-1 from 290 to 390°C and charges a 375/305°C salt store through a counterflow oil–salt heat exchanger. In both plants the receiver is kept above T_{min} + 12 K when the field is not collecting, and electricity for this heating is drawn from generation or imported from the grid on an hourly ledger.

2.1. Site, weather and pressure counterfactual

The site is Golmud (36.42° N, 94.90° E, 2801 m). A licensed Solargis typical meteorological year (TMY)[27] supplies hourly direct normal irradiance (DNI), ambient temperature and wind speed. Annual DNI is 1898 kWh m^{-2}, mean ambient temperature is 7.1°C, the minimum is

−18.8°C and 2550 h are below 0°C. The TMY timestamps are local standard time at the end of each interval, and solar geometry is evaluated at the interval midpoint. An idealised REST2 clear-sky year[28] at a constant 10°C and 3 m s^{-1} serves as a resource counterfactual.

To isolate air density, the pressure experiment changes only the air-property elevation between 0 and 2801 m. Weather, solar geometry, optics, sky temperature and equipment rating are unchanged. Pressure follows the U.S. standard atmosphere[29],

$$p(z) = 101325\,(1 - 2.25577 \times 10^{-5} z)^{5.25588}, \qquad \rho = \frac{p(z)}{287.05\,T}, \tag{1}$$

so that density at 2801 m is 0.710 of its sea-level value at the same temperature. Sky temperature follows Swinbank[30] in all cases.

2.2. Collector loop and receiver

The loop is 600 m long, made of four 150 m assemblies with a 5.77 m aperture (3462 m^2). Absorbed power per unit length is

$$q'_{abs} = DNI\, W \cos\theta\, \rho_m \gamma \tau_g \alpha_a c_{clean} K_{IAM}(\theta)\, \eta_{end}(\theta), \tag{2}$$

with mirror reflectance 0.935, collection factor 0.92, glass transmittance 0.96, absorptance 0.955, cleanliness 0.95 and the EuroTrough incidence-angle modifier. The receiver uses an absorber–glass two-node balance based on the Forristall model[31], with radiative transfer across the evacuated annulus and convection plus radiation from the glass to the environment. External convection uses the Churchill–Bernstein cross-flow correlation[32] with Sutherland air viscosity[33], and internal convection uses the laminar limit or the Dittus–Boelter correlation[34]. The overall structure follows established trough performance models[35]. Absorber emittance is $0.062 + 2.00 \times 10^{-7} T_a^2$ (T_a in °C), following the PTR70 characterisation[36]. Each nonlinear receiver solution must close its heat balance to within 10^{-4} W m^{-1}.

The field runs at variable flow to reach 540°C for salt and 390°C for oil from a common 290°C cold header. Heat loss along the loop follows an axial enthalpy march,

$$\dot{m}\frac{dh}{dx} = q'_{abs} - q'_{loss}(T), \qquad h(T) = \int_{T_c}^{T} c_p(\theta)\, d\theta, \tag{3}$$

solved with a midpoint predictor–corrector on 16 segments. Flow is bounded between 0.5 and 60 kg s^{-1}: if the target outlet cannot be reached at minimum flow, collection stops; if it is exceeded at maximum flow, the field defocuses. Collection also requires DNI $\geq$ 50 W m^{-2}, solar zenith

below 88° and incidence below 75°. The solar energy input $E_{sun} = A \sum_t DNI_t \Delta t$ counts every hour, including hours rejected by these gates.

2.3. Storage and power block

All annual cases use a solar multiple of 2.5. The power-block thermal rating is the field's design-point output (900 W m^{-2}, normal incidence, 25°C, 3 m s^{-1}) divided by 2.5, which gives 0.859 MW$_{th}$ and 0.340 MW$_e$ net for salt and 0.898 MW$_{th}$ and 0.298 MW$_e$ for oil. Storage is a fixed-temperature reservoir,

$$E_{t+1} = E_t + E_{ch} - E_{dis} - E_{TES \to rec} - E_{loss}, \qquad 0 \le E_t \le E_{cap}, \tag{4}$$

starting empty. Direct salt storage operates between 540 and 290°C. For oil, one 15 K counterflow approach on every exchanger end fixes the salt tanks at 375/305°C, the charge-side oil return at 320°C and discharged oil at 360°C. Only the pinch-feasible part of excess field enthalpy can be stored; the rest is counted as dumped return heat at the cold header. Tank loss is set to 1.5% of capacity per day at the reference hot-to-ambient temperature difference and is met first from stored heat and then by electric heating.

When field and storage supply the power block together, the mixed inlet enthalpy is the mass-weighted mean of the two streams. Gross efficiency is 0.74 of the Carnot efficiency between a turbine-inlet temperature 28 K below the HTF supply and 45°C condensation; a fixed 10% parasitic fraction gives net output. Receiver and tank heating are counted separately from this fraction. Storage discharges in all non-valley hours. This dispatch rule is a simple heuristic rather than an optimised schedule.

2.4. Receiver maintenance policies and electricity ledger

When the field is not collecting, the receiver must stay above a guard temperature $T_g = T_{min} + 12$ K. The baseline T_{min} is 238°C for Solar Salt and 12°C for VP-1. Three policies are compared:

1. *Steady*: the receiver heat loss at T_g is supplied electrically in every non-collecting hour.
2. *Thermal inertia*: a lumped receiver inventory of fluid and metal cools from the cold-header temperature on a 300 s internal step, and heating starts only when it reaches T_g. Before collection resumes, solar heat must reheat the inventory to 290°C; this start-up debit is subtracted from delivered heat.

3. *Inertia with storage supply*: as policy 2, but the heating demand is met from storage when the storage delivery temperature exceeds T_g; this heat is then unavailable for generation.

Electric heating is assumed to convert electricity to heat at unity efficiency. A receiver-off case, which ignores freeze protection, is computed as an explicit counterfactual. For lower T_{min}, the Solar Salt sensible-property correlation is retained and extrapolated; no phase change, draining or supercooling credit is modelled.

At each hour the ledger separates generation, on-site heating, export and import:

$$E_{exp,t} = \max(E_{gen,t} - E_{heat,t}, 0), \qquad E_{imp,t} = \max(E_{heat,t} - E_{gen,t}, 0). \tag{5}$$

2.5. Cost model and exergy indicator

Capital cost comprises the field at 1200 CNY m^{-2}, storage at 155 CNY kWh_{th}^{-1}, an oil–salt exchanger increment of 140 CNY kWh_{th}^{-1} for the indirect plant, and the power block at 7.8×10^6 CNY MW_e^{-1} of net rating. Annual O&M is 2% of capital, project life 30 years and discount rate 8%. These values form a common screening basis rather than traced procurement prices; Section 4.6 checks the storage values against current raw-material prices, and Section 4.5 varies them. With annualised cost $C_a = CAPEX\,(CRF + 0.02)$, two conventions are reported:

$$LCOE_{net} = \frac{C_a}{E_{exp} - E_{imp}}, \qquad LCOE_{exp} = \frac{C_a + \sum_t p_t E_{imp,t}}{E_{exp}}. \tag{6}$$

The net-energy convention charges imported electricity at the plant's own cost; the export convention buys it at the tariff p_t of 1.2/0.6/0.3 CNY kWh^{-1} for peak, flat and valley hours (peak 10:00–13:00 and 18:00–21:00; valley 23:00–06:00). The tariff is illustrative, not a contracted Golmud price. Solar exergy follows Petela[37], and the design-point stream exergy increment is $\Delta\dot{B} = \dot{m} \int_{T_c}^{T_h} c_p(T)(1 - T_0/T)\,dT$.

2.6. Parity search and cost scan

The parity temperature is the T_{min} at which the lowest salt levelized cost over the storage candidates equals the lowest oil levelized cost. Storage candidates are every integer hour from 0 to 12 h; the reporting matrix in Table 2 also uses a coarser 0/3/6/9/12 h grid. T_{min} is scanned from 90 to 240°C in 1 K steps on a pre-computed library of annual results. Each bracketed crossing is then refined with Brent's method on the full annual model, to 0.01 K and a cost residual below 0.01 CNY MWh^{-1}. To test cost sensitivity, the salt and oil storage cost bases are

multiplied independently by 0.5, 0.75, 1, 1.25, 1.5, 2 and 3, giving 49 combinations under each of the two conventions. Storage duration is re-selected for every combination and temperature. A combination with no crossing in 90–240°C is reported as such; this finite scan does not prove that no crossing exists outside it.

3. Model verification

The receiver model was compared with the 11 measured heat-loss points of the PTR70 test[36], matching the measured absorber temperature at each point (Fig. 2, left). The mean absolute difference is 3.29 W m^{-1} and the maximum is 12.38 W m^{-1}. Because the emittance correlation comes from the same receiver class, this is a calibration-consistency check rather than an independent validation.

Axial discretisation converges quickly at design irradiance (Fig. 2, right). With the power-block rating frozen, 8 and 16 segments differ in annual net electricity by −0.073% for salt and −0.001% for oil, and the parity temperature on the five-level storage grid moves by 0.43 K. Near the 50 W m^{-2} collection cutoff, 4 and 16 segments differ by up to 5.59% in instantaneous useful heat; 16 segments are therefore used throughout. The storage ledger closes to within 9.5×10^{-7} J per hourly step in all 103 annual cases, and receiver standby heating changes by about 1% between 600 and 60 s internal steps.

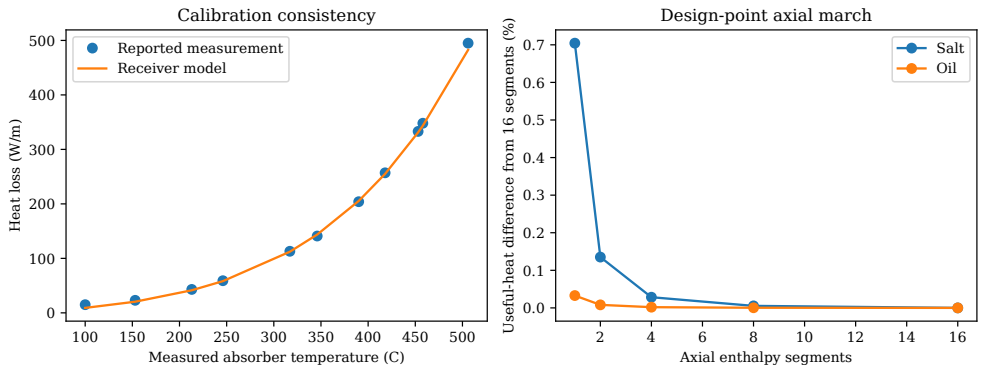


Figure 2: Model checks. Left: receiver heat loss against the 11 PTR70 measurements (calibration consistency). Right: design-point useful heat relative to the 16-segment solution versus the number of axial segments.

At the direct-delivery design point the solar exergy account closes (Fig. 3). Net electricity is 29.3% of incident solar exergy for salt and 25.7% for oil. The salt plant's higher delivery

temperature therefore gives it a clear design-point advantage, which the annual results below must overcome.

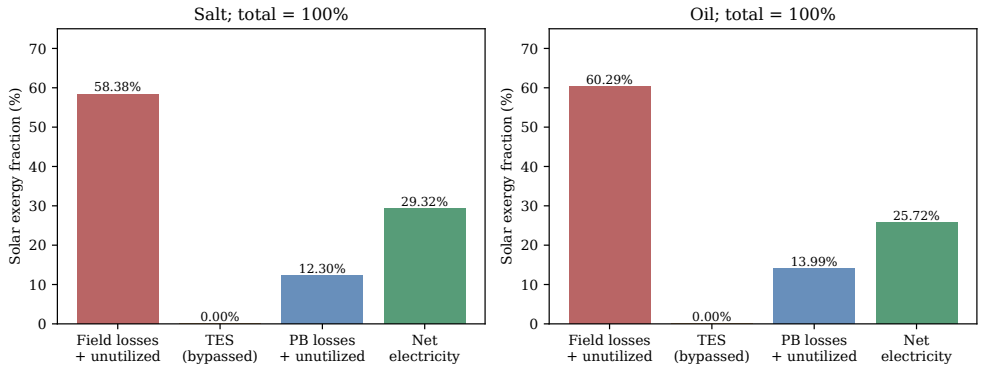


Figure 3: Design-point solar exergy account with direct delivery (storage bypassed). Field and power-block bars include both losses and unutilised exergy leaving the boundary.

4. Results

4.1. The freeze-protection burden, not air density, drives the site effect

With steady maintenance, the 6 h salt plant uses 206.5 MWh of electricity per year to keep its receiver at 250°C; the 3 h oil plant uses 5.7 MWh. This salt demand equals 18.4% of the net output the same plant would deliver without freeze protection (1120.8 MWh). It is nearly constant through the year, between 16.1 and 18.3 MWh per month (Fig. 4), because the receiver is held about 250 K above ambient in every season. The oil demand is small and seasonal, from 0.23 MWh in July to 0.74 MWh in December and January.

Air density matters much less. Moving the air properties from 0 to 2801 m with fixed weather changes the salt plant's annual net output from 913.30 to 914.32 MWh (+0.11%) and its receiver heating from 206.73 to 206.48 MWh. The oil plant's net output changes from 977.75 to 977.74 MWh. Lower density reduces external convection from the glass envelope, but in an evacuated receiver this term is small next to the freeze-protection demand. At this site the relevant altitude effect is therefore the cold climate and long non-collecting hours, not the thin air.

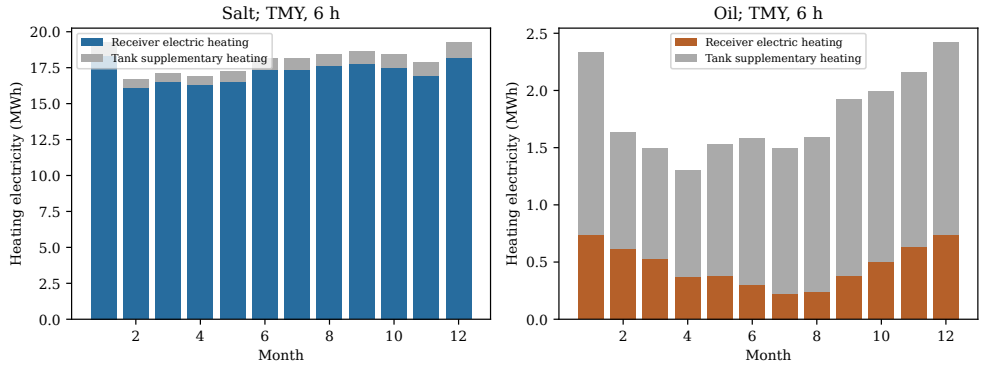


Figure 4: Monthly heating electricity for the 6 h designs on the Golmud TMY under steady maintenance. Receiver heating and supplementary tank heating are shown separately.

4.2. Annual ranking and storage duration

Table 2 and Fig. 5 show how freeze protection reverses the ranking. Under clear-sky weather with no receiver maintenance, salt is 16% cheaper than oil. On the TMY without maintenance, salt is still 12% cheaper (738.7 against 840.9 CNY MWh^{-1}). Steady maintenance raises the salt cost to 905.5 CNY MWh^{-1} but changes the oil cost only from 840.9 to 846.0 CNY MWh^{-1}, so oil becomes 6.6% cheaper. Re-optimising storage over integer hours moves the oil optimum from 3 to 2 h (843.7 CNY MWh^{-1}) and keeps the salt optimum at 6 h; the ranking does not change. Scaling the optical input by ±5% does not change it either: at +5%, salt (6 h) costs 856.9 and oil (3 h) 822.5 CNY MWh^{-1}.

Table 2: Lowest net-energy levelized cost on the 0/3/6/9/12 h storage grid.

Weather / receiver maintenance	HTF	Storage (h)	Net output (MWh)	$LCOE_{net}$ (CNY MWh^{-1})
Clear sky / off	Salt	6	1905.7	434.5
Clear sky / off	Oil	3	1532.0	516.9
TMY / off	Salt	6	1120.8	738.7
TMY / off	Oil	3	941.8	840.9
TMY / steady	Salt	6	914.3	905.5
TMY / steady	Oil	3	936.2	846.0

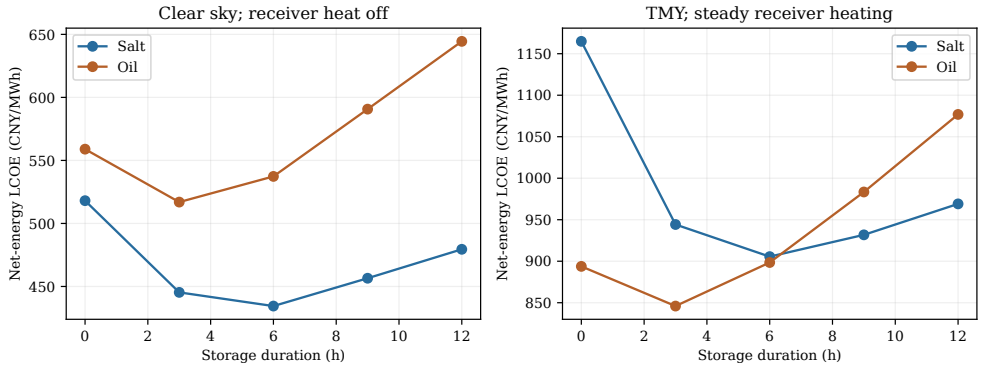


Figure 5: Net-energy levelized cost against storage duration. Left: clear-sky counterfactual without receiver maintenance. Right: Golmud TMY with steady receiver maintenance.

4.3. Maintenance policy and electricity accounting

How the receiver is kept warm changes the gap but, under the net-energy convention, not the ranking (Fig. 6). Allowing the receiver to cool on its thermal inertia lowers the salt cost from 905.5 to 892.9 CNY MWh^{-1} (6 h), and supplying the remaining demand from storage lowers it further to 872.3 CNY MWh^{-1}, because 33.7 MWh of stored heat replaces electric heating. For oil the inertia policy is worse than steady heating (866.5 against 846.0 CNY MWh^{-1} at 3 h): its standby loss is small, but reheating the cooled inventory before each start costs 91.3 MWh of solar heat per year.

The accounting convention matters more. Under the export convention, imported electricity is bought at the time-of-use tariff, which is mostly the valley or flat price at night, rather than at the plant's own cost. Salt then costs 843.9 CNY MWh^{-1} with steady maintenance and 825.3 CNY MWh^{-1} with inertia and storage supply, against 841.7 CNY MWh^{-1} for oil. The best salt option is therefore 2% cheaper than the best oil option under the export convention and 3% more expensive under the net-energy convention. A ranking at this site is only meaningful once the accounting rule is stated.

4.4. The parity freezing limit

Lowering the minimum operating temperature lowers the guard temperature and with it the steady receiver loss. Figure 7 shows the result on the hourly storage candidates. The salt lower envelope reaches the 2 h oil optimum at T_{min} = 196.5°C, 41.5 K below the 238°C baseline. On

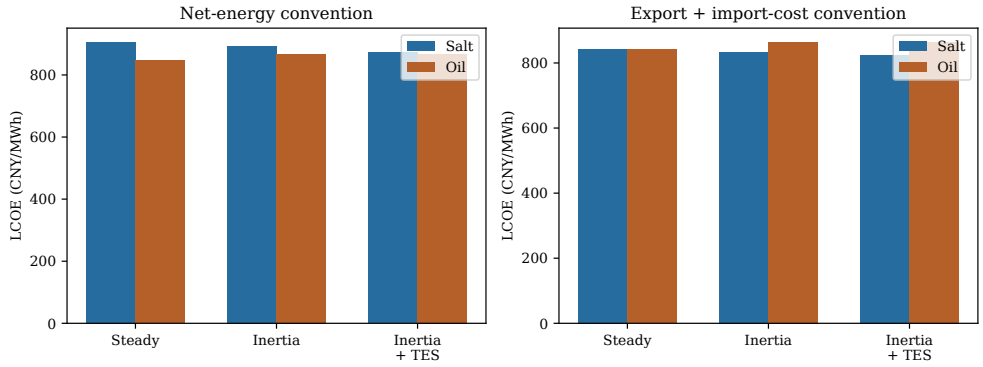


Figure 6: Levelized cost by receiver-maintenance policy for the 6 h salt and 3 h oil designs under the net-energy (left) and export-based (right) conventions.

the coarser five-level grid, with a 3 h oil comparator, the crossing is at 198.4°C, so the storage discretisation shifts the target by 1.9 K. Under the export convention the crossing is at 234.2°C, only 3.8 K below the baseline, consistent with the near-parity found above.

The right panel of Fig. 7 converts the same curves into an allowable change in annualised system cost, $\delta C_a/C_a = LCOE_{oil}/LCOE_{salt} - 1$, at unchanged output. At $T_{min} = 90$°C salt could carry about 10% more annualised cost and still match oil. At 238°C it would need about 7% less. This allowance applies to the whole system cost, not to the salt price alone; Section 4.6 converts it into a salt price.

4.5. Sensitivity of the target and the storage optimum to storage cost

Storage cost moves both the optimal storage duration and the parity temperature. With inherited costs, the salt optimum is 5–6 h over the scanned temperatures, and the leading candidates lie within 0.1% of each other (Fig. 8a). Across the 49 net-energy cost combinations, the salt optimum ranges over 2, 4, 5 and 6 h and the oil optimum over 0–4 h (Fig. 8b). The export convention adds 7 h for salt. No combination selects more than 7 h for salt or 4 h for oil, so the 12 h upper bound is never active. At a solar multiple of 2.5 and these cost levels, the plants favour short storage, unlike the large-storage cases in which Dersch et al. found Solar Salt competitive[21].

Figure 9 maps the parity temperature over the cost combinations. Of the 98 combinations and conventions, 61 have a crossing between 90 and 240°C. In 25 the salt envelope is cheaper throughout the scanned range and in 12 the oil envelope is cheaper throughout. Under the net-

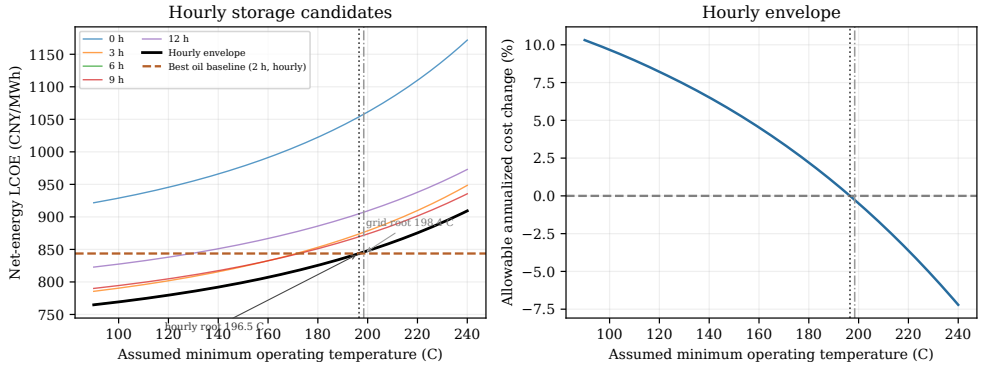


Figure 7: Effect of the assumed minimum operating temperature of the salt. Left: net-energy levelized cost of selected storage durations, their hourly lower envelope and the best oil design (2 h); vertical lines mark the hourly (196.5°C) and five-level (198.4°C) parity temperatures. Right: allowable change in annualised system cost relative to the best oil design.

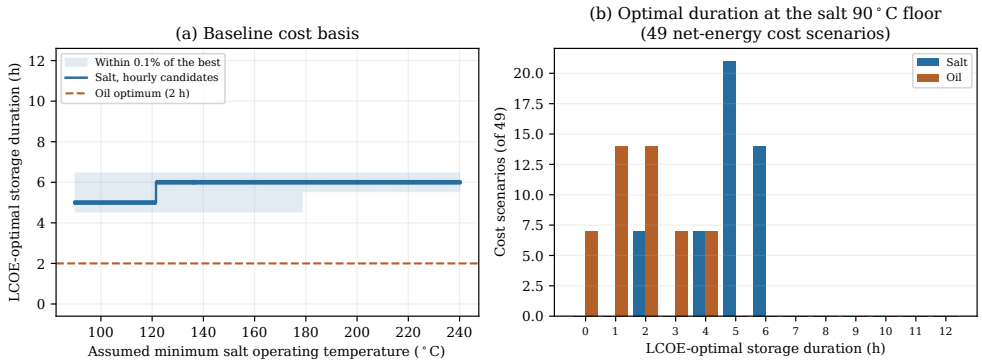


Figure 8: Cost-optimal storage duration. (a) Salt optimum over the hourly candidates against the assumed minimum operating temperature, with the band within 0.1% of the best and the oil optimum. (b) Distribution of the optimum over the 49 net-energy cost combinations, evaluated at the 90°C scan floor.

energy convention, halving the salt storage cost basis raises the target from 196.5 to 230.1°C, so Solar Salt itself almost suffices; a 1.5-fold increase lowers it to 160.1°C and doubling to 119.2°C. A 1.5-fold increase in the oil storage basis raises the target to 218.2°C. The target is therefore as sensitive to the storage cost of the indirect oil plant as to that of the salt plant.

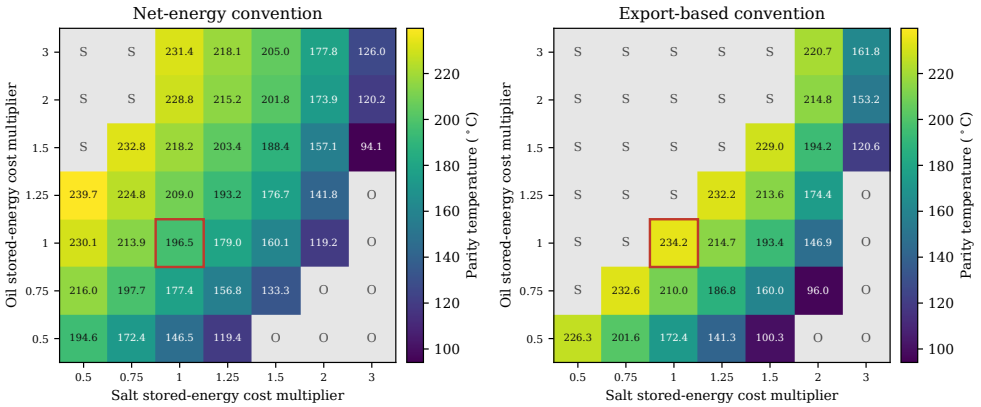


Figure 9: Parity minimum operating temperature over the salt (columns) and oil (rows) storage-cost multipliers, under the net-energy (left) and export-based (right) conventions. S or O: no crossing in 90–240°C because the salt (S) or oil (O) envelope is cheaper throughout. The outlined cell is the inherited cost basis.

4.6. A ternary-salt-like window and the raw-material check

Real low-melting salts trade a lower freezing limit for a lower upper limit. Commercial ternary $Ca(NO_3)_2$–KNO_3–$NaNO_3$ mixtures are typically operated between about 170 and 500°C[21, 12]. Table 3 therefore adds a case with a 500°C hot side and T_{min} = 170°C, computed with the same model and storage re-optimised over 0–12 h. The Solar Salt sensible-property correlation is retained, so this is a ternary-salt-like window rather than a model of a specific product.

The lower hot side alone helps slightly: at 238°C, a 500°C field costs 889.5 against 905.5 CNY MWh^{-1} at 540°C, because lower receiver losses outweigh the lower cycle efficiency. With a 500°C hot side the parity temperature rises from 196.5 to 207.3°C. The ternary-like window at 170°C lies 37 K below that target and gives 804.2 CNY MWh^{-1}, 4.7% below oil. Under the export convention the 500°C salt envelope is cheaper than oil over the whole 90–240°C range. This agrees with Dersch et al., who found the ternary salt cheapest at all their sites[21].

Table 3: Effect of the salt operating window (Golmud TMY, steady maintenance). The allowance is $LCOE_{oil}/LCOE_{salt} - 1$ against the 2 h oil optimum (843.7 CNY MWh^{-1} net, 840.1 CNY MWh^{-1} export).

Salt window (hot / T_{min}, °C)	Storage (h)	LCOE$_{net}$ (CNY MWh^{-1})	LCOE$_{exp}$ (CNY MWh^{-1})	Allowance (net)	Parity T_{min} (net, °C)
540 / 238 (Solar Salt)	6	905.5	843.9	−6.8%	196.5
500 / 238	6[a]	889.5	831.2	−5.1%	207.3
500 / 170 (ternary-like)	5	804.2	780.5	+4.9%	–

[a]Best of 3, 6 and 9 h. The 500°C parity temperature uses hourly candidates.

The inherited storage cost can be compared with current raw-material prices. A domestic quotation of 4.10 CNY kg^{-1} for nitrate salt was used; it does not specify grade, tax or delivery terms. With the model's sensible-enthalpy integral, a 540/290°C direct store holds 378.6 kJ per kilogram of salt, or 9.51 kg kWh$_{th}^{-1}$, which is 39 CNY kWh$_{th}^{-1}$ of salt, or 25% of the 155 CNY kWh$_{th}^{-1}$ basis. The 375/305°C indirect store holds only 105.1 kJ kg^{-1}, so it needs 34.3 kg kWh$_{th}^{-1}$ and 140 CNY kWh$_{th}^{-1}$ of salt, 48% of its 295 CNY kWh$_{th}^{-1}$ basis. Both shares are plausible for two-tank storage, where tanks, insulation, foundations and heat exchangers make up the rest[16, 38]. Because the indirect store needs 3.6 times more salt per unit of stored energy, a change in salt price changes the oil plant's storage cost more than the salt plant's. This is one reason why the parity target in Fig. 9 responds to the oil cost basis.

The same calculation gives a price allowance for the ternary-like window. Its 4.9% allowance corresponds to 0.37 million CNY of extra capital for the 5 h plant. Its 500/290°C store needs 11.3 kg kWh$_{th}^{-1}$, so the 4363 kWh$_{th}$ store holds 49.5 t of salt, 8.0 t more than a 540°C store of equal capacity; the flat 155 CNY kWh$_{th}^{-1}$ basis does not price that extra salt. After deducting it, the allowance would still tolerate a ternary salt price of about 10.8 CNY kg^{-1}, 2.6 times the Solar Salt quotation, if all extra cost were in the storage inventory. Salt in the field piping and receivers is not costed separately in the model, so this is an upper estimate.

5. Discussion

5.1. What sets the target

The salt plant's freeze-protection demand is almost independent of season (Fig. 4). It is set by how many hours the field is idle and by how far the guard temperature lies above ambient, and at

250°C the guard term dominates. A cold winter adds only a few percent to this demand, whereas the oil demand triples. Lowering the freezing limit therefore acts on the largest term, which explains why the parity target is a temperature and why it lies at about 197°C rather than close to ambient. The same mechanism makes storage-supplied maintenance attractive, as Dersch et al. also recommend[21]. In this plant, however, storage supply alone does not close the gap under the net-energy convention.

5.2. Implications for salt development

For a salt to be useful at this site, its *operating* minimum, including the guard margin and the liquidus or crystallisation temperature, must lie below roughly 197°C for a 540°C plant, or 207°C for a 500°C plant. A low melting onset is not enough: Bonk et al. report a quaternary salt with a melting onset of 99.4°C but a liquidus of 136.3°C, with stability limited to about 500°C[17], and a quinary nitrate/nitrite mixture shows crystallisation values that drift upward from 122.4 to about 129.5°C after thermal cycling[19]. On those figures, several published low-melting candidates would pass the temperature target with margin. Whether they are worthwhile then depends on their upper limit, long-term stability, corrosion behaviour and price. The ternary-like case suggests that a salt operating between 170 and 500°C could cost up to about 2.6 times as much as Solar Salt in the storage inventory and still break even with oil at Golmud.

5.3. Limitations

The plant is a one-loop equivalent (0.34 MW_e) with costs scaled linearly; a utility-scale plant adds fixed costs, header and piping inventory, and start-up effects that may change the comparison[39]. The power block uses a fixed fraction of Carnot efficiency, and the oil–salt exchanger is pinch-feasible but has no UA or pressure-drop design. Receiver maintenance uses a lumped inventory without joints, headers or heat-tracing zones, and no draining or freeze-recovery strategy is modelled. The capital costs are a screening basis; the raw-material check supports their order of magnitude but not a procurement estimate. Salt properties below 238°C are extrapolated from the Solar Salt correlation. Finally, one TMY does not cover inter-annual or extreme-cold variability. The receiver model is consistent with laboratory heat-loss data, but field measurements of freeze-protection electricity would be needed to confirm the absolute demand.

6. Conclusions

An hourly model of a one-loop parabolic-trough plant at Golmud compared direct Solar Salt with thermal oil and indirect salt storage under electric freeze protection. The main findings are:

1. Steady electric receiver maintenance costs the 6 h salt plant 206.5 MWh per year, 18.4% of its output without freeze protection, against 5.7 MWh for oil. This reverses a 12% salt advantage into a 6.6% oil advantage in net-energy levelized cost (905.5 against 846.0 CNY MWh^{-1}).
2. Air-density effects at 2801 m change annual output by only 0.11%. The site effect comes from the freeze-protection burden, which is nearly constant through the year.
3. With storage re-optimised over hourly candidates, salt matches oil when its minimum operating temperature falls to 196.5°C (net-energy convention) or 234.2°C (export convention). Across 98 cost and accounting combinations, 61 have a parity temperature between 90 and 240°C, and the cost-optimal storage stays between 0 and 7 h.
4. Thermal-inertia operation and storage-supplied maintenance reduce the salt cost to 872.3 CNY MWh^{-1}; under the export convention they make salt 2% cheaper than oil.
5. A ternary-salt-like window of 170–500°C gives 804.2 CNY MWh^{-1}, 4.7% below oil, and would tolerate a storage salt price of about 10.8 CNY kg^{-1}, 2.6 times the Solar Salt quotation used here.

These figures give material developers a concrete target and show that storage cost, maintenance policy and electricity accounting must be stated alongside any claim that a salt is cheaper than oil at a cold site.

Nomenclature

A	Aperture area (m^2)
C_a	Annualised fixed cost (CNY yr^{-1})
CRF	Capital recovery factor
E	Energy (MWh)
h	Specific sensible enthalpy (J kg^{-1})
$\dot{B}$	Exergy rate (W)
$\dot{m}$	Mass flow (kg s^{-1})
p_t	Electricity tariff in hour t (CNY kWh^{-1})
T_c, T_h, T_g	Cold, hot and guard temperatures
T_{min}	Minimum operating temperature of the HTF
LCOE	Levelized cost of electricity (CNY MWh^{-1})
TES	Thermal energy storage
TMY	Typical meteorological year

Declaration of generative AI and AI-assisted technologies in the writing process

During the preparation of this work the authors used ChatGPT and Claude to assist with code development, computational checks, figure preparation and language editing. After using these tools, the authors reviewed and edited the content as needed and take full responsibility for the content of the publication.

CRediT authorship contribution statement

Zhaohui Han: Conceptualization, Methodology, Formal analysis, Visualization, Writing – original draft. **Zengli Dai:** Supervision, Resources, Funding acquisition, Writing – review & editing. **Yuan Wei:** Methodology, Supervision, Project administration. **Yu Xie:** Investigation, Software, Writing – review & editing. **Dongxiang Wang:** Validation, Data curation, Writing – review & editing.

Declaration of competing interest

The authors are employed by SEPCOIII Electric Power Construction Co., Ltd. This research was funded by POWERCHINA GROUP (grant number DJ-ZDXM-2025-19), the parent com-

pany of SEPCOIII. The authors declare no other competing interests.

Funding

This research was funded by POWERCHINA GROUP, grant number DJ-ZDXM-2025-19.

Data availability

The model source code, configuration and derived results are available at `https://github.com/han348661657/msptc` and archived at Zenodo (`https://doi.org/10.5281/zenodo.20896806`); the version used for this article is tagged `paper-a-tsep-2026`. The hourly Solargis TMY is licensed and is not redistributed; an equivalent TMY can be supplied through the `-tmy-file` option for a replacement-weather run. An earlier version of this work was posted as a preprint (`https://doi.org/10.31224/7442`).

References

[1] S. A. Kalogirou, Solar thermal collectors and applications, Progress in Energy and Combustion Science 30 (3) (2004) 231–295. doi:10.1016/j.pecs.2004.02.001.

[2] H. Price, E. Lüpfert, D. Kearney, E. Zarza, G. Cohen, R. Gee, R. Mahoney, Advances in parabolic trough solar power technology, Journal of Solar Energy Engineering 124 (2) (2002) 109–125. doi:10.1115/1.1467922.

[3] A. Fernández-García, E. Zarza, L. Valenzuela, M. Pérez, Parabolic-trough solar collectors and their applications, Renewable and Sustainable Energy Reviews 14 (7) (2010) 1695–1721. doi:10.1016/j.rser.2010.03.012.

[4] U. Herrmann, D. W. Kearney, Survey of thermal energy storage for parabolic trough power plants, Journal of Solar Energy Engineering 124 (2) (2002) 145–152. doi:10.1115/1.1467601.

[5] D. Kearney, U. Herrmann, P. Nava, B. Kelly, R. Mahoney, J. Pacheco, R. Cable, N. Potrovitza, B. Blake, H. Price, Assessment of a molten salt heat transfer fluid in a parabolic trough solar field, Journal of Solar Energy Engineering 125 (2) (2003) 170–176. doi:10.1115/1.1565087.

[6] K. Vignarooban, X. Xu, A. Arvay, K. Hsu, A. M. Kannan, Heat transfer fluids for concentrating solar power systems – a review, Applied Energy 146 (2015) 383–396. doi:10.1016/j.apenergy.2015.01.125.

[7] A. Giaconia, A. C. Tizzoni, S. Sau, N. Corsaro, E. Mansi, A. Spadoni, T. Delise, Assessment and perspectives of heat transfer fluids for CSP applications, Energies 14 (22) (2021) 7486. doi:10.3390/en14227486.

[8] A. Bonk, T. Bauer, Solar salt – thermal property analysis – extended version, Tech. rep., German Aerospace Center (DLR) (2022). doi:10.57676/3rea-p782.

[9] M. Mehos, H. Price, R. Cable, D. Kearney, B. Kelly, G. Kolb, F. Morse, Concentrating solar power best practices study, Tech. Rep. NREL/TP-5500-75763, National Renewable Energy Laboratory (2020). doi:10.2172/1665767.

[10] National Solar Thermal Power Industry Technology Innovation Strategic Alliance and China Renewable Energy Society, Blue book of China's concentrating solar power industry, Advanced Technology of Electrical Engineering and Energy 45 (2) (2025) 1–45. doi:10.12067/ATEEE2601019.

[11] B. Lynch, H. Metghalchi, Y. Levendis, Concentrating solar thermal power in China: 2025 review and outlook, ASME Open Journal of Engineering 4 (2025) 040807. doi:10.1115/1.4070013.

[12] N. Dicke, M. Meyer-Grünefeldt, M. Wittmann, J. Stengler, P. Horta, P. Martins, et al., Demonstration of 3.5 MWth parabolic trough with ternary molten salt at the Évora molten salt platform, in: SolarPACES Conference Proceedings, Vol. 1, 2024. doi:10.52825/solarpaces.v1i.640.

[13] T. Kotzab, N. Dicke, M. Wittmann, M. Meyer-Grünefeldt, J. Stengler, P. Martins, P. Horta, T. Hirsch, Controller tests for molten salt parabolic trough systems with loop-wise control valves, in: SolarPACES Conference Proceedings, Vol. 3, 2025. doi:10.52825/solarpaces.v3i.2334.

[14] V. Russo, G. Napoli, F. Rovense, P. Di Ascenzi, G. Giorgi, L. Mongibello, C. Cancro, G. Ciniglio, W. Gaggioli, Investigations on solidification and melting processes of the solar

salt mixture in evacuated and non-evacuated receiver tubes, Energies 18 (17) (2025) 4492. doi:10.3390/en18174492.

[15] C. Prieto, A. Blindu, L. F. Cabeza, J. Valverde, G. García, Molten salts tanks thermal energy storage: Aspects to consider during design, Energies 17 (1) (2024) 22. doi:10.3390/en17010022.

[16] B. Kelly, D. Kearney, Thermal storage commercial plant design study for a 2-tank indirect molten salt system, Tech. Rep. NREL/SR-550-40166, National Renewable Energy Laboratory (2006).

[17] A. Bonk, M. Braun, T. Bauer, Phase diagram, thermodynamic properties and long-term isothermal stability of quaternary molten nitrate salts for thermal energy storage, Solar Energy 231 (2022) 1061–1071. doi:10.1016/j.solener.2021.12.020.

[18] H. Wang, J. Wei, L. Luo, J. Wang, J. Xu, J. Yin, S. Ma, G. Zhao, Thermophysical properties and phase diagram analysis of binary, ternary and quaternary nitrates for thermal energy storage applications, Solar Energy 286 (2025) 113151. doi:10.1016/j.solener.2024.113151.

[19] Y. Wang, Y. Lu, Y. Wang, Y. Wu, Q. Gao, C. Zhang, Investigation on thermal performance of quinary nitrate/nitrite mixed molten salts with low melting point for thermal energy storage, Solar Energy Materials and Solar Cells 270 (2024) 112803. doi:10.1016/j.solmat.2024.112803.

[20] Y. Wang, Y. Lu, Y. Wu, C. Zhang, Phase diagram analysis and thermophysical properties investigation of mixed molten salts with low liquid operating temperature for thermal energy storage, Energy 333 (2025) 137386. doi:10.1016/j.energy.2025.137386.

[21] J. Dersch, M. K. Wittmann, T. Hirsch, Comparison of molten salts and thermal oil in parabolic trough power plants for different sites and different storage capacities, Energies 18 (2) (2025) 326. doi:10.3390/en18020326.

[22] N. Khandelwal, P. S. Yadav, Z. Said, M. Sharma, A. K. Shukla, O. Singh, D. Khandelwal, H. Caliskan, A comprehensive analysis of energy, exergy, economic and environment on

integrated solar-combined cycle with various htfs and thermal storage, Applied Energy 376 (2024) 124203. doi:10.1016/j.apenergy.2024.124203.

[23] Z. Said, M. Ghodbane, B. Boumeddane, A. K. Tiwari, L. S. Sundar, C. Li, N. Aslfattahi, E. Bellos, Energy, exergy, economic and environmental (4e) analysis of a parabolic trough solar collector using MXene based silicone oil nanofluids, Solar Energy Materials and Solar Cells 239 (2022) 111633. doi:10.1016/j.solmat.2022.111633.

[24] S. K. Singh, A. K. Tiwari, Z. Said, MXene nanofluid enhanced parabolic trough collectors: An integrated energy, exergy, environmental, and economic study, Solar Energy 276 (2024) 112658. doi:10.1016/j.solener.2024.112658.

[25] D. Wang, B. Fan, Y. Chen, Y. Han, Y. Liu, Y. Wang, H. Liu, X. Jiao, Comparative analysis of heat loss performance of flat plate solar collectors at different altitudes, Solar Energy 244 (2022) 490–506. doi:10.1016/j.solener.2022.08.060.

[26] P. Alamdari, M. Khatamifar, W. Lin, Heat loss analysis review: Parabolic trough and linear fresnel collectors, Renewable and Sustainable Energy Reviews 199 (2024) 114497. doi:10.1016/j.rser.2024.114497.

[27] S. Wilcox, W. Marion, Users manual for TMY3 data sets, Tech. Rep. NREL/TP-581-43156, National Renewable Energy Laboratory (2008). doi:10.2172/928611.

[28] C. A. Gueymard, REST2: High-performance solar radiation model for cloudless-sky irradiance, illuminance, and photosynthetically active radiation – validation with a benchmark dataset, Solar Energy 82 (3) (2008) 272–285. doi:10.1016/j.solener.2007.04.008.

[29] NOAA and NASA and USAF, U.s. standard atmosphere, 1976, Tech. Rep. NOAA-S/T 76-1562, U.S. Government Printing Office (1976).

[30] W. C. Swinbank, Long-wave radiation from clear skies, Quarterly Journal of the Royal Meteorological Society 89 (381) (1963) 339–348. doi:10.1002/qj.49708938105.

[31] R. Forristall, Heat transfer analysis and modeling for a parabolic trough solar receiver implemented in engineering equation solver, Tech. Rep. NREL/TP-550-34169, National Renewable Energy Laboratory (2003). doi:10.2172/15004820.

[32] S. W. Churchill, M. Bernstein, A correlating equation for forced convection from gases and liquids to a circular cylinder in crossflow, Journal of Heat Transfer 99 (2) (1977) 300–306. doi:10.1115/1.3450685.

[33] W. Sutherland, The viscosity of gases and molecular force, Philosophical Magazine 36 (223) (1893) 507–531. doi:10.1080/14786449308620508.

[34] F. P. Incropera, D. P. DeWitt, T. L. Bergman, A. S. Lavine, Fundamentals of Heat and Mass Transfer, 7th Edition, John Wiley & Sons, 2011.

[35] M. J. Wagner, P. Gilman, Technical manual for the SAM physical trough model, Tech. Rep. NREL/TP-5500-51825, National Renewable Energy Laboratory (2011). doi:10.2172/1016437.

[36] F. Burkholder, C. Kutscher, Heat loss testing of schott's 2008 PTR70 parabolic trough receiver, Tech. Rep. NREL/TP-550-45633, National Renewable Energy Laboratory (2009). doi:10.2172/1369635.

[37] R. Petela, Exergy of undiluted thermal radiation, Solar Energy 74 (6) (2003) 469–488. doi:10.1016/S0038-092X(03)00226-3.

[38] P. Kurup, C. S. Turchi, Parabolic trough collector cost update for the system advisor model (SAM), Tech. Rep. NREL/TP-6A20-65228, National Renewable Energy Laboratory (2015). doi:10.2172/1227713.

[39] S. Akar, P. Kurup, Parabolic trough collector cost update for industrial process heat in the United States, in: Proceedings of EuroSun 2024, International Solar Energy Society, 2024. doi:10.18086/eurosun.2024.04.01.